Solvent Effects on the Oxidative Electrochemical Behavior of *cis*-Bis(isothiocyanato)ruthenium(II)-bis-2,2′-bipyridine-4,4′-dicarboxylic Acid

Francesca Cecchet,[†] Anna Maria Gioacchini,[†] Massimo Marcaccio,[†] Francesco Paolucci,*[,†] Sergio Roffia,[†] Monica Alebbi,[‡] and Carlo Alberto Bignozzi*[,‡]

Dipartimento di Chimica G. Ciamician, Università di Bologna, Via Selmi 2, 40126 Bologna, Italy, and Dipartimento di Chimica, Università di Ferrara, via L. Borsari, 46, 44100 Ferrara, Italy

Received: November 29, 2001; In Final Form: February 3, 2002

The redox properties of *cis*-[Ru(dcbpyH$_2$)$_2$(NCS)$_2$] ([Ru(dcbpyH$_2$)$_2$(NCS)$_2$]; dcbpyH$_2$ = 2,2′-bipyridine- 4,4′-dicarboxylic acid) have been investigated in various solvents by combining electrochemical techniques (cyclic voltammetry (CV) and spectroelectrochemistry), mass spectrometry, digital simulation techniques, and semiempirical quantum chemical calculations. The electrochemical study has shown that while in polar solvents such as acetonitrile and ethanol the complex undergoes, following oxidation, the rapid loss of SCN ligands, forming the corresponding solvato complexes. In the less polar solvent tetrahydrofuran, a reversible oxidative CV behavior is observed at relatively low scan rates. On the basis of the CV and spectroelectrochemical studies and supported by quantum chemical calculations, a complex parallel ECE mechanism is proposed, comprising the loss of the SCN ligands in their pristine (anionic) form, which is initiated by the metal-centered oxidation process.

Introduction

Thin film photoelectrochemical solar devices based on dye-sensitized wide band gap semiconductors are considered an attractive alternative to solid-state silicon cells.[1] The principles of functioning of the photoelectrochemical devices have been previously described,[2] and the fundamental steps are summarized in Scheme 1.

The molecular sensitizer (S), which is adsorbed on the surface of the semiconductor, has the role of absorbing visible photons, thus giving rise to fast and efficient charge injection from an electronically excited state (S*) to the conduction band. The regenerative step that follows involves the nascent oxidized form (S^+) and a reducing agent such as iodide dissolved in a suitable solvent.

Despite intense efforts in many laboratories to design organic dyes[3] and inorganic complexes based on Fe^{II},[4] Ru^{II},[5] Re^{I},[6] Pt^{II},[7] and Os^{II} [8] metal ions, the most interesting candidate for practical application is still the [Ru(dcbpyH$_2$)$_2$(NCS)$_2$] complex, the preparation of which dates back to 1993.[9] The important advantages in the use of this complex are the availability of a simple synthetic chemistry,[9] the ultrafast electron injection (<100 fs) from the charge-transfer excited state to the conduction band of the semiconductor,[10] and the solar-to-electric power-conversion yield, which has been reported to be on the order of 10%.[9] Studies that have focused on the degradation of solar cells based on this complex have shown that the type of solvent and the purity of the different cell components are crucial parameters for obtaining long-term stability.[11] With these parameters standardized, the only source of instability should be related to kinetic competition between charge injection and photochemical reactions from S* and to competition between thermal reactions of S^+ and bimolecular electron transfer with iodide. Although the photochemical studies rule out the possibility that excited-state chemical processes compete with ultrafast charge-injection processes,[10] it is still unclear if the chemical reactivity of S^+ is relevant to cell instability. We wish to report here the results of electrochemical, spectroelectrochemical, and quantum chemical studies on [Ru(dcbpyH$_2$)$_2$(NCS)$_2$] in different solvents, which allow us to gain insight into the kinetics of chemical processes originating from the oxidized dye.

SCHEME 1

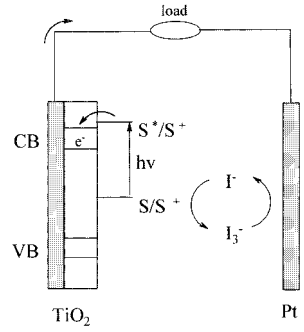

Results and Discussion

Cyclic Voltammetry. The cyclic voltammetry (CV) curve for a saturated (≤0.3 mM) [Ru(dcbpyH$_2$)$_2$(NCS)$_2$] ACN solution at 25 °C and 10 V/s (Figure 1a) displays three oxidation peaks (A, B, and C), with peak potentials of 0.92, 1.25, and 1.76 V, respectively. A cathodic counterpart is observed only for peaks B and C at 1.16 and 1.71 V, respectively, whereas under the conditions of Figure 1, peak A is fully irreversible. At higher scan rates and when the potential scan was limited to peak A (see Figure 1b), a cathodic counterpart of peak A was observed, although the cathodic-to-anodic peak ratio was always lower than 1 at any scan rate (up to 1000 V/s). Under these

* To whom correspondence should be addressed. E-mail: paolucci@ciam.unibo.it or g4s@dns.unife.it.
[†] Università di Bologna.
[‡] Università di Ferrara.

10.1021/jp014343a CCC: $22.00
Published on Web 03/23/2002

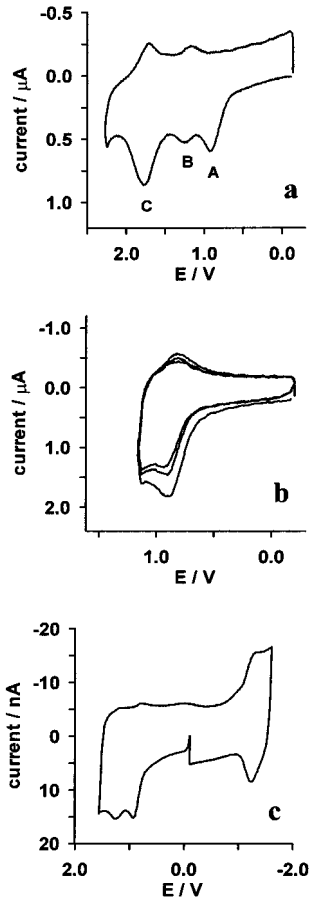

Figure 1. CV curves for a saturated $[Ru(dcbpyH_2)_2(NCS)_2]$, 0.05 M TEAH, ACN solution. (a) $\upsilon = 10$ V/s, (b) $\upsilon = 100$ V/s, and (c) $\upsilon = 300$ V/s, $T = 25$ °C; working electrode, Pt disk UME: (a) and (b) 125 μm, (c) 10 μm diameter.

conditions, $E_{1/2}$ was estimated to be 0.85 V, in agreement with earlier reported values.[2f,9,12]

The three anodic peaks in Figure 1a show different heights; in particular, the height of peak B is significantly lower than that of A or C. Furthermore, the relative peak ratios were significantly affected by changes of scan rate; as the scan rate was increased (up to 1000 V/s), the B/A peak current ratio also increased (from 0.4 to 0.9).[13] At the same time, peak C was found to be complicated by adsorption phenomena because its peak current increased almost linearly with scan rate, which is also suggested by the small distance between peak C and its cathodic counterpart (50 mV under the conditions of Figure 1a).[14] The number of electrons exchanged at peaks A and B was evaluated by comparison with the reduction peak observed in the region of negative potentials (Figure 1c). It has been recently shown that the reduction of $[Ru(dcbpyH_2)_2(NCS)_2]$ at platinum electrodes involves the deprotonation of the $dcbpyH_2$ ligands, followed by the reduction of H^+.[15] Because at least two protons are removed in the process,[15] the reduction peak in Figure 1c corresponds to a two-electron process. By comparison,[13] the overall charge exchanged at peaks A and B also corresponds to two electrons, which means that more than one electron is exchanged at peak A, as was also confirmed by chronoamperometric experiments carried out at an ultramicroelectrode (see Experimental Section) and by bulk electrolysis experiments (vide infra). Finally, one electron is assumed to be exchanged at peak C, although the corresponding charge is difficult to evaluate because of the adsorption contribution to the faradaic current.

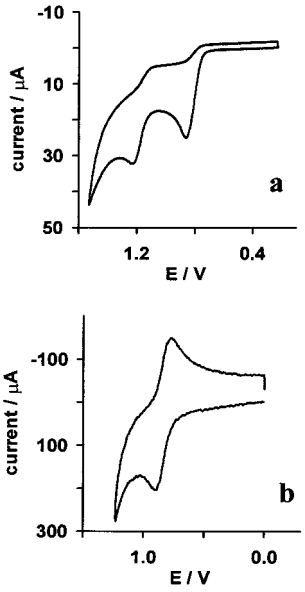

Figure 2. CV curves for 0.5 mM $[Ru(dcbpyH_2)_2(NCS)_2]$. (a) 0.05 M TEAH, ethanol solution; $\upsilon = 0.1$ V/s and (b) 0.05 TBAH, THF solution; $\upsilon = 10$ V/s. $T = 25$ °C; working electrode, Pt wire.

CV investigations were also carried out in ethanol and THF. The CV curve of a 0.5 mM $[Ru(dcbpyH_2)_2(NCS)_2]$ ethanol solution at 25 °C and 0.1 V/s is shown in Figure 2a.

Because of the narrower potential window available in this solvent, only two oxidation peaks are observed, both irreversible, with $E_p = 0.86$ and 1.22 V, respectively. By contrast with the previous case, the two peaks show comparable heights at any scan rate, and both correspond to one electron/molecule. Very different CV behavior was finally observed in THF. Figure 2b shows the CV curve of a 0.5 mM $[Ru(dcbpyH_2)_2(NCS)_2]$ THF solution at 25 °C and 10 V/s, whichdisplays only a single, reversible oxidation peak with $E_{1/2} = 0.84$ V. Similar reversible anodic behavior was also reported recently in other solvents such as DMF, although only at higher scan rates ($\upsilon \geq 1000$ V/s), and acetone, where, however, the CV curve was heavily distorted by adsorption phenomena.[12a] Such a reversible oxidation peak was attributed to the conversion of Ru(II) to Ru(III),[12] and the same attribution can be safely made for the first oxidation peak in the CV curves of Figures 1 and 2a. In the latter case, however, the oxidation process is irreversible; therefore, peaks B and C in Figures 1a and 2a represent oxidations involving novel species yielded by the follow-up reaction coupled to the metal-centered oxidation A.[16] The chemical, photochemical, and electrochemical oxidative degradations of $[Ru(dcbpyH_2)_2(NCS)_2]$ and related compounds have long been debated in view of their immediate consequences on the long-term stability of photoelectrochemical solar cells.[9,11,12,17] Analogous to that proposed for other complexes that contain easily oxidized ligands (the $E_{1/2}$ value for the $(SCN)_2/SCN^-$ redox couple is, in fact, 0.53 V in ACN[18]), a mechanism was proposed that accounts for the observed instability of $[Ru(dcbpyH_2)_2(NCS)_2]^+$ and comprises, following the metal-centered oxidation, (i) fast intramolecular electron transfer from $-$NCS to Ru(III) and (ii) the release of the oxidized ligand, (i.e., radical $NCS^\bullet$ substituted by a solvent molecule (mechanism I, Scheme 2).[19]

According to such a mechanism, the metal would then retain its +2 oxidation state, and the irreversible oxidative process would involve the NCS group rather than the metal, which is in agreement with the fact that the HOMO (as calculated for the model complex $[Ru(bpy)_2(NCS)_2]$[20]) is largely localized onto

SCHEME 2

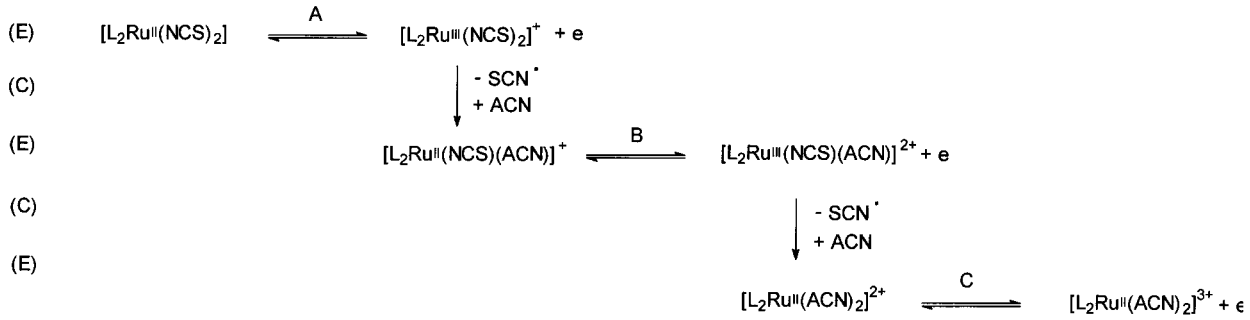

the NCS ligands. According to mechanism I, the removal of both −NCS ligands would occur only sequentially: the first oxidation would, in fact, yield (in ACN) the stable solvato complex $[Ru^{II}(dcbpyH_2)_2(NCS)(ACN)]^+$ that is oxidized only at more positive potentials (vide infra), thus allowing the removal of the second −NCS ligand. The inference is that peaks A and B should each correspond to the exchange of one electron; therefore, they should always display equal heights (i.e., a CV pattern that is the same as that observed in ethanol). Then, unequal peak heights as found in ACN or the reversible behavior observed in THF and other solvents suggests the need for a reappraisal of the electrode mechanism to also include possible solvent effects.

As a first step toward a revised mechanism, quantum chemical calculations on the title complex and its oxidized form were carried out using the semiempirical PM3(tm) method.[21] This method is believed to give a reliable theoretical description of the above species on the basis of the study carried out on the model species $[Ru(bpy)_2(NCS)_2]$ and $[Ru(bpy)_2(NCS)_2]^+$ with various methods (i.e., PM3(tm), DFT pBP/DN*[22] (implemented in the Spartan program[23]) and ab initio HF/3-21G*[24] (using the GAMESS (US) program[25])). The geometries of the model species obtained with the three methods were very similar to one another and were in agreement with the reported data.[26] The dipole moments and the relevant molecular orbitals obtained by the three methods were also very similar. The optimized geometry at the DFT level of $[Ru(bpy)_2(NCS)_2]$ and $[Ru(bpy)_2(NCS)_2]^+$ was obtained, and the HOMO of the neutral species is shown in Figure 3a.

In line with previous calculations,[20] the HOMO shows a large contribution from the two −NCS ligands and to a lesser extent, from the Ru orbitals. Only slight differences in the Ru atom contribution to the HOMO calculated with the different methods were found: with PM3(tm), such a contribution to the HOMO is smaller than that with the other two methods (Figures 1S, 2S, Supporting Information). Importantly, the results of the calculations carried out on $[Ru(bpy)_2(NCS)_2]^+$ contrast with the observed labilization of the Ru−NCS bond induced by the oxidation. The removal of one electron from $[Ru(bpy)_2(NCS)_2]$ does not induce dramatic geometry changes and brings about the shortening (by 0.04 Å) rather than the elongation of the Ru−NCS bonds, along with the increase of the SCN−Ru−NCS angle by 1.6° and the nearly unchanged N−C−S angle. PM3(tm) calculations carried out on $[Ru(dcbpyH_2)_2(NCS)_2]$ (Figure 4) and $[Ru(dcbpyH_2)_2(NCS)_2]^+$ provided similar results: the oxidation process produces the shortening of the Ru−NCS bond by 0.06 Å and a minor change (0.2°) in the SCN−Ru−NCS angle.

Calculations then suggest that the Ru−NCS bonds are unlikely to dissociate spontaneously after the oxidation; rather, they predict reversible oxidative behavior such as that observed in THF. Inner-sphere ion−solvent interactions, not included in the calculations, may, however, be responsible for a decrease of the chemical stability of the oxidized complex. We propose an alternative to mechanism I where the elongation of the Ru−NCS bond is concerted with the approach of a nucleophilic solvent molecule to within bonding distance, thus favoring a process disallowed in vacuum. The calculation of the reacting system, including the solvent molecules, along the reaction pathway remains outside the limits of our theoretical approach. However, it is possible and deemed important within the

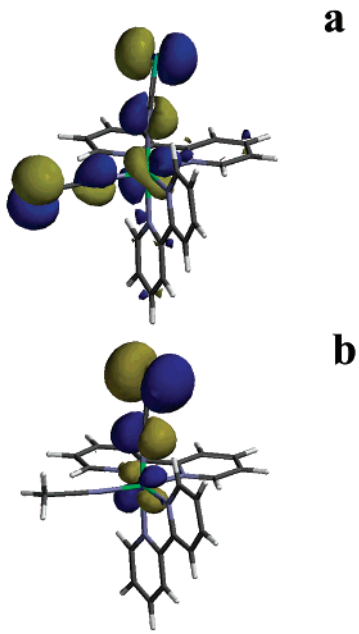

Figure 3. Molecular orbital surfaces calculated at the DFT level of theory. (a) HOMO of the model species *cis*-$[Ru(bpy)_2(NCS)_2]$ (optimized geometry) and (b) HOMO of the model solvato complex $[Ru(bpy)_2(NCS)(ACN)]^+$ (optimized geometry).

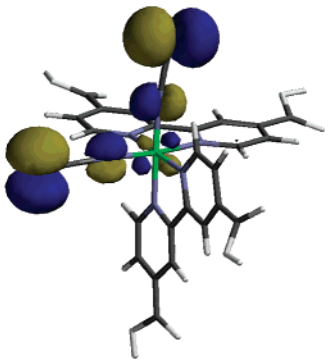

Figure 4. HOMO surface calculated at the PM3(tm) level of theory for *cis*-$[Ru(dcbpyH_2)_2(NCS)_2]$ (optimized geometry).

TABLE 1: PM3(tm) Charge Variation over the −NCS Ligand as a Function of the Ru−NCS Bond Elongation for *cis*-[Ru(dcbpyH$_2$)$_2$(NCS)$_2$] and Its Oxidized Form *cis*-[Ru(dcbpyH$_2$)$_2$(NCS)$_2$]$^+$

Δr_{Ru-NCS}/Å	[Ru(dcbpyH$_2$)$_2$(NCS)$_2$]	[Ru(dcbpyH$_2$)$_2$(NCS)$_2$]$^+$
0.1	−0.06	−0.02
0.2	−0.12	−0.06
0.3	−0.18	−0.95

SCHEME 3

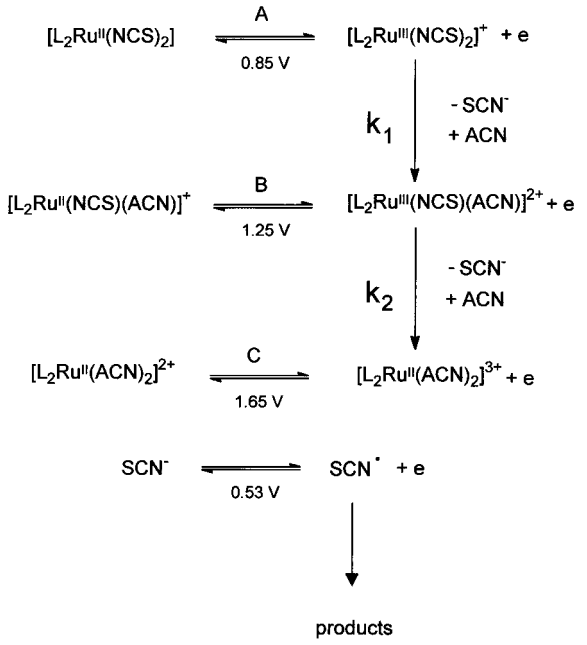

concerted mechanism to appraise the evolution of the electronic charge distribution in the oxidized complex when the Ru−NCS bond is elongated to some extent with respect to the optimized length. A similar procedure was recently adopted to describe the C−Cl bond cleavage occurring during the electrochemical reduction of a fullerene derivative, $C_{60}Ph_5Cl$.[27] In Table 1, the results of the calculations carried out on [Ru(dcbpyH$_2$)$_2$(NCS)$_2$] and on its oxidized form [Ru(dcbpyH$_2$)$_2$(NCS)$_2$]$^+$ are reported: when the Ru−NCS bond is elongated by 0.1−0.3 Å, a negative variation of the ligand total charge, located especially on the N atom, develops in [Ru(dcbpyH$_2$)$_2$(NCS)$_2$], and such an effect is even more dramatic in the oxidized form. This result suggests that thiocyanate leaves the oxidized complex (replaced by a solvent molecule) in its pristine, anionic form, whereas the metal keeps the +3 oxidation state (mechanism II, Scheme 3).

Notice that both of the resulting species (i.e., SCN^- and [Ru^{III}(dcbpyH$_2$)$_2$(NCS)(ACN)]$^{2+}$) are unstable at potentials close to that of peak A (0.92 V). $E_{1/2}$[$(SCN)_2/SCN^-$] is 0.53 V;[18] SCN^- can therefore be oxidized as soon as it is released from the complex. On the other hand, Ru^{II} is more difficult to oxidize in the solvato complex than in the pristine complex; using Lever's parameters[28] and the $E_{1/2}$ value for [Ru^{III}(dcbpyH$_2$)$_2$(NCS)$_2$]$^+$/[Ru^{II}(dcbpyH$_2$)$_2$(NCS)$_2$] (0.85 V), the estimated $E_{1/2}$ value for the [Ru$^{III/II}$(dcbpyH$_2$)$_2$(NCS)(ACN)]$^{2+/+}$ redox couple is 1.25 V. This result is in line with the calculations carried out on [Ru(bpy)$_2$(NCS)(ACN)]$^+$ (Figure 3b) and [Ru(dcbpyH$_2$)$_2$(NCS)-(ACN)]$^+$ that show lower HOMO energies than in [Ru(bpy)$_2$-(NCS)$_2$] and [Ru(dcbpyH$_2$)$_2$(NCS)$_2$], respectively. At potentials close to peak A, the newly formed solvato complex [Ru^{III}-(dcbpyH$_2$)$_2$(NCS)(ACN)]$^{2+}$ would therefore be reduced, yielding the stable species [Ru^{II}(dcbpyH$_2$)$_2$(NCS)(ACN)]$^+$ (Scheme 3). If the two processes (i.e., SCN^- oxidation and [Ru^{III}(dcbpyH$_2$)$_2$-

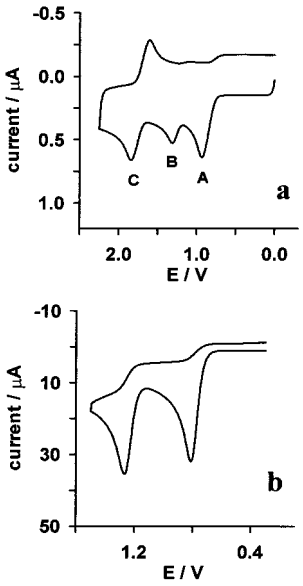

Figure 5. Simulated CV curves for [Ru(dcbpyH$_2$)$_2$(NCS)$_2$] under the conditions of Figures 1a and 2a, calculated according to the mechanism described in Scheme 3 (mechanism II). See text for simulation parameters.

(NCS)(ACN)]$^{2+}$ reduction) occur simultaneously at the electrode, because of their opposite valences they would give no contribution to the overall current: peak A would then still correspond to the exchange of one electron/molecule (i.e., that corresponding to the primary oxidation of pristine [Ru(dcbpyH$_2$)$_2$-(NCS)$_2$][29]). The ensuing [Ru^{II}(dcbpyH$_2$)$_2$(NCS)(ACN)]$^+$ would be oxidized at peak B and loose the second −NCS ligand by a similar mechanism to that outlined above, thus still exchanging one electron/molecule and obtaining [Ru^{II}(dcbpyH$_2$)$_2$(ACN)$_2$]$^{2+}$ (and SCN$^•$). The latter complex would finally be oxidized at peak C (the expected $E_{1/2}$, evaluated using Lever's parameters, is 1.65 V). As long as peaks A and B have equal heights, both corresponding to one electron/molecule, such a mechanism may adequately describe the CV behavior that is observed in ethanol or in ACN at high scan rates. As such, mechanism II is not distinguishable from mechanism I. On the other hand, if the loss of the second −NCS ligand is fast with respect to [Ru^{III}-(dcbpyH$_2$)$_2$(NCS)- (ACN)]$^{2+}$ reduction (Scheme 3), then [Ru^{III}-(dcbpyH$_2$)$_2$(ACN)$_2$]$^{3+}$ (and another SCN^-) would form at potentials close to peak A, which would then correspond to the exchange of two electrons (one for each released SCN^-). Intermediate charges of peak A between 1 and 2 electrons/molecule are expected when the above two processes (i.e., the reduction of [Ru^{III}(dcbpyH$_2$)$_2$(NCS)(ACN)]$^{2+}$ and the release of the −NCS ligand from it) have comparable time scales. In such a case, only residual [Ru^{II}(dcbpyH$_2$)$_2$(NCS)- (ACN)]$^+$ would contribute to peak B; peak B would correspond to less than 1 electron/molecule, which is the behavior observed in ACN at relatively low scan rates.

The digital simulation of the CV curves obtained under the conditions of Figures 1a and 2a, calculated according to mechanism II, is shown in Figure 5a, b. Rather good agreement with the experimental curves was obtained. In the simulation, the $E_{1/2}$ values obtained by employing Lever's parameters (see above) were used, and the following kinetic parameters (at 298 K) were obtained by fitting procedures: $k_1 = 5 \times 10^3$ s^{-1} (ACN); 200 s^{-1} (ethanol); $k_2 = 4 \times 10^3$ s^{-1} (ACN); 5 s^{-1} (ethanol). Furthermore, a relatively fast chemical degradation of SCN$^•$ was also included in the simulation to account for the

absence of a cathodic peak attributable to $SCN^{\bullet}$ reduction[30] in the CV curves in Figures 1 and 2

The concerted mechanism II provides a rationale for the observed solvent effects on the stability of $[Ru(dcbpyH_2)_2(NCS)_2]^+$. Two oppositely charged species are formed by the cleavage of the Ru−NCS bond vis-à-vis the positive/neutral couple formed according to mechanism I. The solvent dielectric properties are therefore expected to affect the stability of $[Ru^{III}(dcbpyH_2)_2(NCS)_2]^+$ greatly, which would explain the reversible CV behavior observed in solvents such as THF and acetone. In more polar solvents, where the separation of the two charged fragments is facilitated, the nucleophilic properties of the solvent are expected to play a major role and would explain the different behavior observed in ACN and ethanol; the solvent ACN molecules would compete more efficiently for the Ru^{III} nucleusthan would the ethanol solvent molecules, allowing the second −NCS release to occur, to some extent, at peak A.

Bulk electrolysis experiments, coupled to spectroscopic and mass spectrometric techniques, confirmed the predictions of mechanism II that both ligands can be lost following the first oxidation of the complex. In both ACN and ethanol, the electrolysis performed at potentials corresponding to peak A consumed more than one electron/molecule. Figure 6 shows the spectral changes recorded during the electrolysis in the two solvents. Only transient isosbestic points could be observed.

In ACN, the initial spectrum shows two bands at 543 and 400 nm that evolve during the electrolysis to a single band at 447 nm. In ethanol, the spectrum of $[Ru(dcbpyH_2)_2(NCS)_2]$ changed from the two initial bands at 530 and 390 nm to a single band at 436 nm. Within a few hours, however, while the ACN solution was stable, the ethanol solution absorbance changed at open-circuit conditions and under an argon atmosphere from the single band at 436 nm to two bands at 490 and 372 nm that were similar although broader than those observed in the pristine $[Ru^{II}(dcbpyH_2)_2(NCS)_2]$ solution (Figure 6c). The final product obtained in ACN was isolated and identified as $[Ru(dcbpyH_2)_2(ACN)_2]^{2+}$ by comparison of its absorption spectrum and CV curve[31] with those of an authentic sample of that species and by electrospray mass spectrometric (ESMS) analysis of the electrolyzed solution. The positive ion mode ES mass spectrum of the product obtained in ACN was dominated by a signal at $m/z = 629$ exhibiting the typical ruthenium isotopic pattern, and no residual signal due to pristine $[Ru(dcbpyH_2)_2(NCS)_2]$ (at $m/z = 948$) was observed. The signal at $m/z = 629$ was assigned to the fragment $[Ru(dcbpyH_2)_2(CH_3CN)]^+$ that would form from the *bis*-acetonitrile complex under ES experimental conditions. Because of its instability in the long time scale, ESMS analysis of the product of the bulk electrolysis in ethanol was performed on samples taken directly from the electrochemical cell during the experiment at various degrees of electrolysis. The mass spectrum showed a complex pattern. However, a signal at $m/z = 648$ showing the isotopic pattern of ruthenium appeared in the spectrum and became the major signal toward the end of the electrolysis. Such a signal was attributed to the ion $[Ru(dcbpyH_2)_2(H_2O)_2 + Na]^+$, likely formed from the presence of residual water in the solvent that was used as received.

Concluding Remarks. This study shows that the instability observed for the oxidized form of $[Ru(dcbpyH_2)_2(NCS)_2]$ in solution is due to substitution of the coordinated −NCS ligands with solvent molecules. Electrochemical reversibility of the Ru(II)/(III) redox couple was observed in the noncoordinating apolar solvent THF, whereas only partial reversibility was observed in ACN at high scan rates. As also suggested by quantum chemical calculations, the ligand(s) loss would occur according to a concerted mechanism in which following the one-electron oxidation of the Ru(II) center the NCS^- ligands are first released as anions and then oxidized while the Ru(III) residue is reduced. The rate constants for the first chemical step involving the oxidized Ru(III) residue is estimated to be on the order of 10^4 s^{-1} (in ACN). This value could be of practical relevance in evaluating the stability of sensitized TiO_2 solar cells, allowing that no difference in dye stability is introduced by dye adsorption on the TiO_2 surface. Considering that the reduction of the photogenerated Ru(III) center on TiO_2 by I^- is essentially diffusion-controlled and occurs on a time scale shorter than 10 ns in the presence of 0.3 M LiI,[2f] chemical reactions originating from the nascent Ru(III) in ACN would be at least 10^4 times slower than chemical reduction by iodide. Similar conclusions may be drawn for ethanol, whereas the reversibility of the oxidation in THF at low scan rates translates into a lifetime

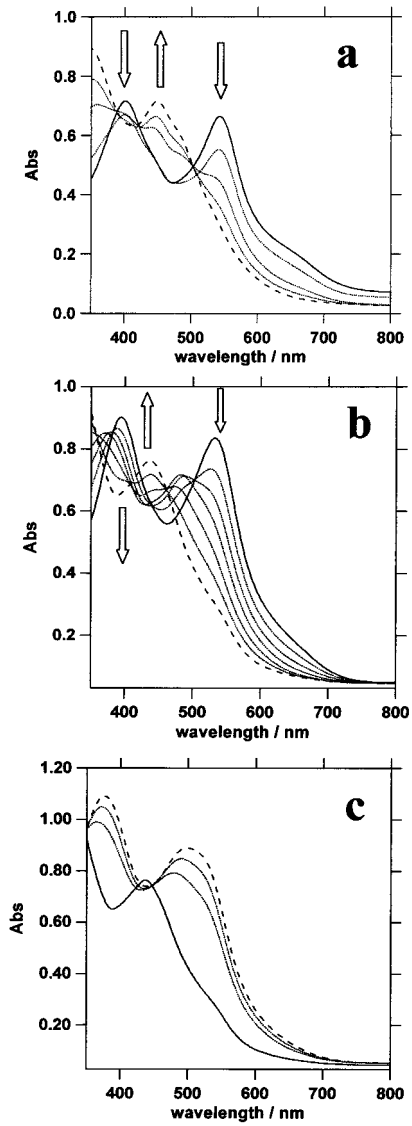

Figure 6. Absorption spectrum changes of (a) saturated $[Ru(dcbpyH_2)_2(NCS)_2]$, 0.05 M TEAH, ACN solution and (b) 0.5 mM $[Ru(dcbpyH_2)_2(NCS)_2]$, 0.05 M TEAH, ethanol solution during electrolysis. Solid line: initial spectrum, dotted lines: intermediate spectra, dashed line: final spectrum. $E_{appl} = 1.0$ V. (c) Absorption spectrum changes of solution (b) after electrolysis. The electrolyzed solution was kept at open circuit conditions and under an argon atmosphere. Solid line: initial spectrum; dotted lines: intermediate spectra; dashed line: final spectrum.

of the $[Ru^{III}(dcbpyH_2)_2(NCS)_2]^+$ radical cation on the order of 10^2 s.

Experimental Section

Materials. Tetrabutylammonium hexafluorophosphate (TBAH, puriss. from Fluka) or tetraethylammonium hexafluoroborate (TEAH, puriss. from Fluka) were used as supporting electrolytes as received. Acetonitrile (ACN, Uvasol, Merck) was refluxed over CaH_2, under argon, vacuum distilled into a Schlenk flask containing activated 3 Å molecular sieves, and kept under vacuum prior to use. Tetrahydrofuran (THF, LiChrosolv, Merck) was treated according to a procedure described elsewhere.[32] Ethanol (puriss. p.a., Fluka) was used as received. For the cyclic voltammetric experiments, the solvent was distilled into the electrochemical cell prior to use using a trap-to-trap procedure.

Preparations. *cis*-$[Ru(dcbpyH_2)_2(NCS)_2]$ was prepared as reported by Nazereruddin.[9] *cis*-$[Ru(dcbpyH_2)_2(Cl)_2]$[9] (100 mg) was dissolved in boiling methanol, and 63 mg of $AgCF_3SO_3$ was added. The solution was kept at reflux for 2 h and then rotary evaporated to dryness. The solid was stirred in 30 mL of acetonitrile and filtered. The dark-red solution was kept at reflux for 6 h and then cooled. The yellow acetonitrile complex was precipitated by addition of ether and dried. The complex was shown to be pure by chromatography on silica gel and by elemental analysis. Anal. Calcd for $[Ru(dcbpyH_2)_2(CH_3CN)_2](CF_3SO_3)_2$: C, 37.11; N, 8.66; H, 2.29. Found: C, 37.62; N, 8.81; H, 2.18. ^{1}H NMR: δ 9.52 d, 1H × 2, $J = 6$ Hz; 9.12 s, 2H; 8.96 s, 2H; 8.35 dd, 2H, $J = 6$ Hz, $J = 2$ Hz; 7.8 d, 2H, $J = 6$ Hz; 7.7 dd, 2H, $J = 6$ Hz, $J = 2$ Hz.

Electrochemical Instrumentation and Measurements. The one-compartment electrochemical cell was of airtight design with high-vacuum glass stopcocks fitted with either Teflon or Kalrez (DuPont) O-rings to prevent contamination by grease. The connections to the high-vacuum line and to the Schlenck flask containing the solvent were obtained by spherical joints also fitted with Kalrez O-rings. The pressure measured in the electrochemical cell prior to performing the trap-to-trap distillation of the solvent was typically $(1.0-2.0) \times 10^{-5}$ mbar. The working electrode consisted either of a 0.6 mm-diameter platinum wire (surface area ≈ 0.15 cm^2) sealed in glass or of a Pt disk ultramicroelectrode (UME) also sealed in glass. The counter electrode consisted of a platinum spiral, and the quasi-reference electrode was a silver spiral. The quasi-reference electrode drift was negligible for the time required by a single experiment. Both the counter and the reference electrodes were separated from the working electrode by ~0.5 cm. Potentials were measured with a ferrocene standard and were always referred to a saturated calomel electrode (SCE). $E_{1/2}$ values correspond to $(E_{pc} + E_{pa})/2$ from CV. For irreversible peaks, the peak potential, E_p, measured at 0.5 V s^{-1} is given. Ferrocene was also used as an internal standard for checking the electrochemical reversibility of a redox couple. The number of electrons corresponding to the electrochemical processes was determined by a chronoamperometric experiment carried out at a Pt disk UME (with radius 12.5 μm) and in which both the transient and the steady-state time regions were investigated, according to a procedure described in ref 33.

Potential-controlled bulk electrolysis was carried out in a three-compartment electrochemical cell with both the SCE reference electrode and the platinum spiral counter electrode separated from the working electrode compartment by sintered glass frits. The working electrode was a large-area platinum gauze. The electrolyzed solution was monitored at intervals during the electrolysis by steady-state voltammetry, and at the same time, UV-Vis-NIR spectra were taken.

Voltammograms were recorded with a AMEL model 552 potentiostat or a custom-made fast potentiostat controlled by either an AMEL model 568 function generator or an ELCHEMA model FG-206F. Data acquisition was performed by a Nicolet model 3091 digital oscilloscope interfaced to a PC. The charge exchanged during bulk electrolysis was measured by a AMEL model 731 digital integrator. Absorption spectra were taken using a VARIAN Cary 5E UV-Vis-NIR spectrophotometer. Temperature was controlled to within 0.1 °C with a Lauda Klein-Kryomat thermostat.

ESMS Measurements. The ion trap mass spectrometer used was an LCQ (Finnigan, San José, CA) equipped with an electrospray ion source, operating in the positive ion mode. The electrospray system employed a 4.3 kV spray voltage and a capillary temperature of 180 °C. The positive ion spectra were collected at a scan rate of 0.5 scan/s.

Digital Simulation of Cyclic Voltammetric Experiments. The CV simulations were carried out by using the DigiSim 3.0 software by Bioanalytical Systems Inc. All the electrochemical steps were considered fast in the simulation, and the chemical rate constants were chosen so as to obtain a visual best fit over a 10^2-fold range of scan rates.

Acknowledgment. The group at the University of Bologna acknowledges partial support from MIUR (Contract N. M. M. 03105353), CNR, and University of Bologna (Funds for Selected Research Topics). Financial support from EU under the Joule III Program, Contract N. JOR3-CT98-7040, is gratefully acknowledged.

Supporting Information Available: The HOMO surface of $[Ru(bpy)_2(NCS)_2]$, calculated at the DFT level, and the SOMO surface of $[Ru(bpy)_2(NCS)_2]^+$, calculated at the HF/3-21G* level of theory. This material is available free of charge via the Internet at http://pubs.acs.org.

References and Notes

(1) *Future Generation Photovoltaic Technologies,* American Institute of Physics Conference Proceedings 404, Denver, CO, 1997; McConnell, R. D., Ed.

(2) (a) Vlachopoulos, N.; Liska, P.; Augustynski, J.; Grätzel, M. *J. Am. Chem. Soc.* **1988**, *110*, 1216. (b) O'Regan, B.; Grätzel, M. *Nature* **1991**, *353*, 737. (c) Grätzel, M. *Comments Inorg. Chem.* **1991**, *12*, 93. (d) Argazzi, R.; Bignozzi, C. A.; Heimer, T. A.; Castellano, F. N.; Meyer, G. J. *Inorg. Chem.* **1994**, *33*, 5741. (e) Lees, A. C.; Evrard, B.; Keyes, T. E.; Vos, J. G.; Kleverlan, C. J.; Alebbi, M.; Bignozzi, C. A. *Eur. J. Inorg. Chem.* **1999**, 2309. (f) Hagfeldt, A.; Grätzel, M. *Acc. Chem. Res*. **2000**, *33*, 269−277.

(3) (a) Bedja, I.; Hotchandani, S.; Carpentier, R.; Fessenden, R. W.; Kamat, P. V. *J. Appl. Phys.* **1994**, *75*, 5444 (b) Cherepy N. J.; Smestad, G. P.; Grätzel, M.; Zhang J. Z. *J. Phys. Chem. B* **1997**, *101*, 9342. (c) Van Hal, P. A.; Wienk, M. M.; Kroon, J. M.; Janssen, R. A. J. *J. Phys. Chem. B* **1999**, *103*, 4352. (d) Sayama, K.; Hara, K.; Tuskagoshi, S.; Abe, Y.; Mori, N.; Satsuski, M.; Suga, S.; Sugihara, H.; Arakawa, H. *Chem. Commun.* **2000**, 1173. (e) Liu, C. Y.; Bard, A. J. *J. Photochem. Photobiol., A* **2000**, *130*, 49.

(4) Ferrere, S.; Gregg, B. A. *J. Am. Chem. Soc.* **1997**, *120*, 8843.

(5) For a recent review, see Bignozzi, C. A.; Argazzi, R.; Kleverlaan, C. J. *Chem. Soc. Rev.* **2000**, *29*, 87.

(6) (a) Argazzi, R.; Bignozzi, C. A.; Heimer, T. A.; Meyer, G. J. *Inorg. Chem.* **1997**, *36*, 2. (b) Hasslemann, G. M.; Meyer, G. J. *J. Phys. Chem B* **1999**, *103*, 7671.

(7) Islam, A.; Sugihara, H.; Hara, K.; Singh, L. P.; Katoh, R.; Yanagida, M.; Takahashi, Y.; Murata, S.; Arakawa, H. *New J. Chem.* **2000**, *24*, 343.

(8) Sauvè, G.; Cass, M. E.; Coia, G.; Doig, S. J.; Lauermann, I.; Pomykal, K.; Lewis, N. S. *J. Phys. Chem. B* **2000**, *104*, 6821.

(9) Nazeeruddin, M. K.; Kay, A.; Rodicio, I.; Humphry-Baker, R.; Muller, E.; Liska, P.; Vlachopoulos, N.; Grätzel, M. *J. Am. Chem. Soc.* **1993**, *115*, 6382.

(10) Tachibana, Y.; Haque, S. A.; Mercer, I. P.; Durant, J. R.; Klug, D. R. *J. Phys Chem. B* **2000**, *104*, 1198−1205.

(11) (a) Kohle, O.; Grätzel, M.; Meyer, A. F.; Meyer, T. B. *Adv. Mater. (Weinheim, Ger.)* **1977**, *9*, 904. (b) Turrion, M.; Macht, B.; Salvador, P.; Tributsch, H. *Z. Phys. Chem.* **1999**, *212*, 51. (c) Grünwald, R.; Tributsch, H. *J. Phys. Chem. B* **1997**, *101*, 2564−2575. (d) Kern, R.; Feber, J.; Hinsch, A.; Kroon, J.; Meyer, A.; Meyer, T.; Niepmann, R.; van Roosmalen, J.; Schill, C.; Uhlendorf, I. *Investigation of the Long-Term Stability of Dye Sensitized Solar Cells*, Abstract XIII, International Conference on Photochemical Conversion and Storage of Solar Energy, July 30−August 4, 2000, Snowmass, CO.

(12) (a) Bond, A. M.; Deacon, G. B.; Howitt, J.; MacFarlane, D. R.; Spiccia, L.; Wolfbauer, G. *J. Electrochem. Soc*. **1999**, *146*, 648−656. (b) Nazeeruddin, M. K.; Zakeeruddin, S. M.; Humphry-Baker, R.; Jirousek, M.; Liska, P.; Vlachopoulos, N.; Shklover, V.; Fisher, C. H.; Grätzel, M. *Inorg. Chem.* **1999**, *38*, 6298−6305. (c) Hou, Y.; Xie, P.; Zhang, B.; Cao, Y.; Xiao, X.; Wang, W. *Inorg. Chem*. **1999**, *38*, 6320−6322.

(13) The evaluation of the B/A charge ratio was carried out by the convolutive technique (ref 14, chapter 6). In the case of peaks A and B of the CV curves in Figure 1, a two-step sigmoidal curve is obtained after convolution, where each step is proportional to the number of electrons exchanged in the corresponding redox process.

(14) Bard, A. J.; Faulkner, L. R. *Electrochemical Methods. Fundamentals and Applications*; Wiley & Sons: New York, 2001.

(15) Wolfbauer, G.; Bond, A. M.; Deacon, G. B.; MacFarlane, D. R.; Spiccia, L. *J. Am. Chem. Soc*. **2000**, *122*, 130−142.

(16) The attribution of peak B entirely to a surface-attached form of $[Ru(dcbpyH_2)_2(NCS)_2]$, as suggested in ref 12a, seems to be unlikely under the present conditions. The typical linear dependence of the peak height on scan rate, as expected for a redox process involving adsorbed species,[14] was in fact not observed. In the present case, adsorption may superimpose, to some extent under our conditions, to the diffusion-controlled processes, thus explaining the less satisfactory agreement with the simulated curves (where adsorption was not taken into account) at the highest scan rates.

(17) Wolfbauer, G.; Bond, A. M.; MacFarlane, D. R. *Inorg. Chem*. **1999**, *38*, 3836−3846;

(18) Oskam, G.; Bergeron, B. V.; Meyer, G. J.; Searson, P. C. *J. Phys. Chem. B* **2001**, *105*, 6867−6873.

(19) $SCN^{\bullet}$ is, in fact, expected to be stable with respect to SCN^- at these potentials.[18] For early examples of complexes with easily oxidized ligands, see (a) Keene, F. R.; Salmon, D. J.; Walsh, J. L.; Abruña, H. D.; Meyer, T. J. *Inorg. Chem*. **1980**, *19*, 1896−1903. (b) Kotz, J. C.; Vining, W.; Coco, W.; Rosen, R.; Dias, A. R.; Garcia, M. H. *Organometallics* **1983**, *2*, 68−79.

(20) (a) Rensmo, H.; Lunell, S.; Siegbahn, H. *J. Photochem. Photobiol., A* **1998**, *114*, 117−124. (b) Rensmo, H.; Sodergren, S.; Patthey, L.; Westermark, K.; Vayssieres, L.; Kohle, O.; Bruhwiler, P. A.; Hagfeldt, A.; Siegbahn, H. *Chem. Phys. Lett.* **1997**, *274*, 51−57.

(21) Cundari, T. R.; Deng, J. *J. Chem. Inf. Comput. Sci.* **1999**, *39*, 376.

(22) Perturbative nonlocal Becke−Perdew method using the DN* numerical basis set, which is similar to 6-31G*. (a) Becke, A. D. *Phys. Rev. A: At., Mol., Opt. Phys.* **1988**, *38*, 3089. (b) Perdew, J. P. *Phys. Rev. B: Solid State* **1986**, *33*, 8822.

(23) Spartan 5.1; Wavefunction, Inc.: Irvine, CA.

(24) (a) Binkley, J. S.; Pople, J. A.; Hehre, W. J. *J. Am. Chem. Soc.* **1980**, *102*, 939. (b) Gordon, M. S.; Binkley, J. S.; Pople, J. A.; Pietro, W. J.; Hehre, W. J. *J. Am. Chem. Soc.* **1980**, *104*, 2797. (c) Dobbs, K. D.; Hehre, W. J. *J. Comput. Chem.* **1987**, *8*, 880.

(25) (a) Ab Initio calculations were performed using PC Gamess v. 6.0 of Gamess(US): Granovsky, A. A. http://classic.chem.msu.su/gran/gamess/index.html. (b) Schmidt, M. W.; Baldridge, K. K.; Boatz, J. A.; Elbert, S. T.; Gordon, M. S.; Jensen, J. J.; Koseki, S.; Matsunaga, N.; Nguyen, K. A.; Su, S.; Windus, T. L.; Dupuis, M.; Montgomery, J. A. *J. Comput. Chem.* **1993**, *14*, 1347. (c) The MO density surfaces were obtained using Molden 3.6 for Windows, developed by G. Schaftenaar, CAOS/CAMM Center Nijmegen: Toernooiveld, Nijmegen, The Netherlands.

(26) Herber, R. H.; Nau, G.; Potenza, J. A.; Schugar, H. J.; Bino, A. *Inorg. Chem.* **1989**, *28*, 938−942.

(27) Birkett, P. R.; Taylor, R.; Watcher, N. K.; Carano, M.; Paolucci, F.; Roffia, S.; Zerbetto, F. *J. Am. Chem. Soc.* **2000**, *122*, 4209.

(28) Lever, A. B. P. *Inorg. Chem*. **1990**, *29*, 1271−1285.

(29) The redox framework describing such a mechanism is that of a parallel ECE process, described in electrochemistry as early as 25 years ago (Ružić, I.; Sobel, H.; Smith, D. E. *J. Electroanal. Chem*. **1975**, *65*, 21). In the present case, the zero-electron pathway, associated to the two parallel and opposite redox processes involving $[Ru^{II}(dcbpyH_2)_2(NCS)_2]$ and $[Ru^{III}(dcbpyH_2)_2(NCS)(ACN)]^{2+}$, respectively, is complicated by the SCN^- oxidation, which is the reason peaks A and B do not drop to zero current. Notice that the homogeneous redox reaction between SCN^- and the Ru^{III} solvato complex should also be taken into account (ECE-DISP competition: Andrieux, C. P., Savéant, J.-M. In *Investigations of Rates and Mechanisms of Reactions*; Bernasconi, C. F., Ed.; Wiley & Sons: New York, 1986; Vol. 6, 4/E, Part 2, Chapter VII, pp 364−367). However, when the bond cleavage is very fast, it occurs very close to the electrode surface to which the two species can diffuse back before reacting with one another.

(30) This is in agreement with the fact that under the conditions of Figure 1 the oxidation of SCN^- (NaNCS) is chemically irreversible, with an i_{pc}/i_{pa} ratio much lower than 1.

(31) $[Ru(dcbpyH_2)_2(CH_3CN)_2](CF_3SO_3)_2]$ is only sparingly soluble in ACN. The CV curve showed a single oxidation peak with $E_p \approx 1.75$ V, and analogously to peak C in the CV curve of $[Ru(dcbpyH_2)_2(NCS)_2]$, the peak was distorted by adsorption phenomena.

(32) Carano, M.; Ceroni, P.; Mottier, L.; Paolucci, F.; Roffia, S. *J. Electrochem. Soc.* **1999**, *146*, 3357.

(33) Ceroni, P.; Paolucci, F.; Paradisi, C.; Juris, A.; Roffia, S.; Serroni, S.; Campagna, S.; Bard. A. J. *J. Am. Chem. Soc.* **1998**, *120*, 5480 and ref 17 therein.